Reweighted Laplace Prior Based Hyperspectral Compressive Sensing for Unknown Sparsity: Supplementary Material

Lei Zhang*†, Wei Wei*†, Yanning Zhang†, Chunna Tian‡, Fei Li†
†School of Computer Science, Northwestern Polytechnical University, Xi'an, 710072, China
‡School of Electronic Engineering, Xidian University, Xi'an, 710071, China
†zhanglei211@mail.nwpu.edu.cn, †{weiweinwpu, ynzhang}@nwpu.edu.cn, ‡chnatian@xidian.edu.cn

This document is the Supplementary Material for the CVPR 2015 paper "Reweighted Laplace Prior Based Hyperspectral Compressive Sensing for Unknown Sparsity", which includes three contents:

- Section1: Derivation of the reweighted Laplace prior.
- Section2: Derivation of the optimization procedure.
- Section3: More experimental results.

1. Derivation of the Reweighted Laplace Prior

In this section, we present the detailed derivation of the intuitive reweighted Laplace prior from the hierarchical structure. For each column $\boldsymbol{y}_i$ in Y, we have

$$
\begin{aligned}
p(\boldsymbol{y}_i) &= \int p(\boldsymbol{y}_i|\boldsymbol{\gamma})\, p(\boldsymbol{\gamma}|\boldsymbol{\kappa}) d\boldsymbol{\gamma} \\
&= \int \frac{\exp\left\{-\frac{1}{2}\boldsymbol{y}_i^T \Sigma_y^{-1} \boldsymbol{y}_i\right\}}{(2\pi)^{n_b/2}\,|\Sigma_y|^{1/2}} \prod_{j=1}^{n_b} \frac{\kappa_j}{2} \exp\left(-\frac{\kappa_j \gamma_j}{2}\right) d\boldsymbol{\gamma} \\
&= \int \frac{\prod_{j=1}^{n_b} \exp\left\{-\frac{y_{ji}^2}{2\gamma_j}\right\} \frac{\kappa_j}{2} \exp\left(-\frac{\kappa_j\gamma_j}{2}\right)}{(2\pi)^{n_b/2}\,|\Sigma_y|^{1/2}} d\boldsymbol{\gamma} \\
&= \prod_{j=1}^{n_b} \int \frac{\kappa_j/2}{(2\pi)^{1/2}} \gamma_j^{-1/2} \exp\left(-\frac{y_{ji}^2 + \kappa_j \gamma_j^2}{2\gamma_j}\right) d\gamma_j \\
&= \prod_{j=1}^{n_b} \frac{\kappa_j^{1/2}}{2} \exp\left(-\sqrt{\kappa_j}|y_{ji}|\right) \int \underbrace{\frac{\left(\frac{\kappa_j}{y_{ji}^2}\right)^{1/(2*2)}}{2\sqrt{\frac{\pi}{2\sqrt{\kappa_j y_{ji}^2}}} \exp\left(-\sqrt{\kappa_j y_{ji}^2}\right)} \gamma_j^{-1/2} \exp\left(-\frac{y_{ji}^2 + \kappa_j\gamma_j^2}{2\gamma_j}\right)}_{\mathcal{GIG}(\gamma_j|\kappa_j, y_{ji}, 1/2)} d\gamma_j \\
&= \frac{\exp\left(-\|K\boldsymbol{y}_i\|_1\right)}{2^{n_b}|K|^{-1}},
\end{aligned}
\tag{1}
$$

where $\Sigma_y = diag\left([\gamma_1, ..., \gamma_{n_b}]^T\right)$[1] is the covariance matrix of Y, $K = diag\left([\sqrt{\kappa_1}, ..., \sqrt{\kappa_{n_b}}]^T\right)$ is the weight matrix and $\mathcal{GIG}\left(\gamma_j|\kappa_j, y_{ji}, 1/2\right)$ represents the pdf of generalized inverse Gaussian distribution. It can be seen that the proposed hierarchical prior results in a reweighted Laplace prior on each column of Y with weight matrix K.

*indicates equal contributions.

[1]For a vector $\boldsymbol{x}$, $diag(\boldsymbol{x})$ denotes a diagonal matrix with elements from $\boldsymbol{x}$. For a matrix X, $diag(X)$ denotes extracting the diagonal elements from X to form a vector.

978-1-4673-6964-0/15/$31.00 ©2015 IEEE

2. Derivation of the Optimization Procedure

In this section, we present the detailed derivation of sparsity learning over $\boldsymbol{\gamma}$ and noise estimation over $\boldsymbol{\lambda}$ in the optimization procedure of the main paper.

2.1. Sparse Signal Recovery: Optimizing for γ

Given Y, $\boldsymbol{\lambda}$ and $\boldsymbol{\kappa}$, the sub-problem over $\boldsymbol{\gamma}$ is derived as

$$\min_{\boldsymbol{\gamma}\geq 0} \|Y\|^2_{\Sigma_y} + \log|\Sigma_{by}| + \sum_{i=1}^{n_b} \frac{\kappa_i\gamma_i - 2\log\kappa_i}{n_p} \tag{2}$$

where $\Sigma_{by} = \Sigma_n + AD\Sigma_y D^T A^T$. According to matrix algebra, we rewrite $\log|\Sigma_{by}|$ term as

$$\begin{aligned}\log|\Sigma_{by}| &= \log\left|\Sigma_n + AD\Sigma_y D^T A^T\right| \\ &= \log\left|I_{m_b} + \Sigma_n^{-1} AD\Sigma_y D^T A^T\right| + \log|\Sigma_n| \\ &= \log\left|\Sigma_y^{-1} + D^T A^T \Sigma_n^{-1} AD\right| + \log|\Sigma_y| + \log|\Sigma_n|,\end{aligned} \tag{3}$$

where $I_{m_b} \in \mathbb{R}^{m_b\times m_b}$ is an identity matrix. Substituting Eq. (3) into Eq. (2) and removing those irreverent terms to $\boldsymbol{\gamma}$, we have a new sub-problem over $\boldsymbol{\gamma}$ as

$$\min_{\boldsymbol{\gamma}} \|Y\|^2_{\Sigma_y} + \log\left|\Sigma_y^{-1} + D^T A^T \Sigma_n^{-1} AD\right| + \log|\Sigma_y| + \frac{1}{n_p}\sum_{i=1}^{n_b}\kappa_i\gamma_i \tag{4}$$

Since the concave function $f\left(\boldsymbol{\gamma}^{-1}\right) = \log\left|\Sigma_y^{-1} + D^T A^T \Sigma_n^{-1} AD\right|$ over $\boldsymbol{\gamma}^{-1} = [\gamma_1^{-1}, ..., \gamma_{n_b}^{-1}]^T$ results in Eq. (4) to be a nonconvex optimization, we utilize a conjugate function in convex optimization [3] to transform this noncovex optimization into a convex one by finding a strict upper bound of $f\left(\boldsymbol{\gamma}^{-1}\right)$

$$f\left(\boldsymbol{\gamma}^{-1}\right) = \log\left|\Sigma_y^{-1} + D^T A^T \Sigma_n^{-1} AD\right| \leq \boldsymbol{z}^T\boldsymbol{\gamma}^{-1} - f^*(\boldsymbol{z}), \forall \boldsymbol{z} \geq 0 \tag{5}$$

where $f^*(\boldsymbol{z})$ is the concave conjugate function of $f\left(\boldsymbol{\gamma}^{-1}\right)$, $\boldsymbol{z} = [z_1, ..., z_{n_b}]^T$. It can be proved that the equation in Eq. (5) only succeeds when

$$\begin{aligned} z_i &= \nabla_{\gamma_i^{-1}} \log\left|\Sigma_y^{-1} + D^T A^T \Sigma_n^{-1} AD\right| \\ &= \mathbf{tr}\left[\left(\Sigma_y^{-1} + D^T A^T \Sigma_n^{-1} AD\right)^{-1} \nabla_{\gamma_i^{-1}}\left(\Sigma_y^{-1} + D^T A^T \Sigma_n^{-1} AD\right)\right] \\ &= \mathbf{tr}\left[\left(\Sigma_y^{-1} + D^T A^T \Sigma_n^{-1} AD\right)^{-1} \nabla_{\gamma_i^{-1}}\left(\sum_{j=1}^{n_b}\frac{\boldsymbol{e}_j\boldsymbol{e}_j^T}{\gamma_i} + D^T A^T \Sigma_n^{-1} AD\right)\right] \\ &= \mathbf{tr}\left[\left(\Sigma_y^{-1} + D^T A^T \Sigma_n^{-1} AD\right)^{-1} \boldsymbol{e}_i\boldsymbol{e}_i^T\right] \\ &= \mathbf{tr}\left[\boldsymbol{e}_i^T\left(\Sigma_y^{-1} + D^T A^T \Sigma_n^{-1} AD\right)^{-1}\boldsymbol{e}_i\right], \end{aligned} \tag{6}$$

where $\boldsymbol{e}_i$ is the ith standard unit vector in $\mathbb{R}^{n_b}$. To decrease the inverse operations in Eq. (6), we use matrix algebra to simplify the formula as

$$\begin{aligned} z_i &= \mathbf{tr}\left[\boldsymbol{e}_i^T\left(\Sigma_y^{-1} + D^T A^T \Sigma_n^{-1} AD\right)^{-1}\boldsymbol{e}_i\right] \\ &= \mathbf{tr}\left\{\boldsymbol{e}_i^T\left[\Sigma_y - \Sigma_y D^T A^T\left(\Sigma_n + AD\Sigma_y D^T A^T\right)^{-1} AD\Sigma_y\right]\boldsymbol{e}_i\right\} \\ &= \mathbf{tr}\left[\boldsymbol{e}_i^T\left(\Sigma_y - \Sigma_y D^T A^T \Sigma_{by}^{-1} AD\Sigma_y\right)\boldsymbol{e}_i\right]. \end{aligned} \tag{7}$$

In summary, the formula of $\boldsymbol{z}$ can be written as

$$\boldsymbol{z} = diag\left(\Sigma_y - \Sigma_y D^T A^T \Sigma_{by}^{-1} AD\Sigma_y\right), \tag{8}$$

Substituting Eq. (5) into Eq. (4), we obtain the revised subproblem

$$\min_{\boldsymbol{\gamma}} \|Y\|_{\Sigma_y}^2 + \boldsymbol{z}^T\boldsymbol{\gamma}^{-1} + \log|\Sigma_y| + \frac{1}{n_p}\sum_{i=1}^{n_b}\kappa_i\gamma_i = \sum_{i=1}^{n_b}\left(\frac{\bar{y}_i^2 + z_i}{\gamma_i} + \log\gamma_i + \frac{\kappa_i\gamma_i}{n_p}\right), \tag{9}$$

where $\bar{y}_i$ denotes the ith element of $\bar{\boldsymbol{y}} = diag(YY^T) = [\bar{y}_1, ..., \bar{y}_{n_b}]^T$. Since $\boldsymbol{\gamma} \geq 0$, the solution of γ_i is

$$\gamma_i^{new} = \frac{\sqrt{4\kappa_i n_p\left(\bar{y}_i^2 + z_i\right) + n_p^2} - n_p}{2\kappa_i}. \tag{10}$$

2.2. Noise Estimation: Optimizing for $\boldsymbol{\lambda}$

With the recovered sparse signal Y and prior parameter $\boldsymbol{\gamma}$, we have the following sub-problem over $\boldsymbol{\lambda}$

$$\min_{\boldsymbol{\lambda}\geq 0}\left\|ADY - \frac{G}{\sqrt{n_p}}\right\|_{\Sigma_n}^2 + \log|\Sigma_{by}| \tag{11}$$

where $\Sigma_{by} = \Sigma_n + AD\Sigma_y D^T A^T$. Similar to the optimization of $\boldsymbol{\gamma}$, we a conjugate function to find the strict upper bound of the concave function $\phi(\boldsymbol{\lambda}) = \log|\Sigma_{by}| = \log\left|\Sigma_n + AD\Sigma_y D^T A^T\right|$ as follows

$$\phi(\boldsymbol{\lambda}) = \log\left|\Sigma_n + AD\Sigma_y D^T A^T\right| \leq \boldsymbol{\alpha}^T\boldsymbol{\lambda} - \phi^*(\boldsymbol{\alpha}), \forall\boldsymbol{\alpha} \geq 0 \tag{12}$$

where $\phi^*(\boldsymbol{\alpha})$ is the concave conjugate function of $\phi(\boldsymbol{\lambda})$, $\Sigma_{by} = \Sigma_n + AD\Sigma_y D^T A^T$, $\Sigma_n = diag(\boldsymbol{\lambda})$ and $\boldsymbol{\alpha} = [\alpha_1, ..., \alpha_{mb}]^T$. It can be proved that the equation of Eq. (12) only succeeds when

$$\alpha_i = \nabla_{\lambda_i}\log\left|\Sigma_n + AD\Sigma_y D^T A^T\right| = \mathbf{tr}\left[\boldsymbol{\xi}_i^T\left(\Sigma_n + AD\Sigma_y D^T A^T\right)^{-1}\boldsymbol{\xi}_i\right] = \mathbf{tr}\left(\boldsymbol{\xi}_i^T\Sigma_{by}^{-1}\boldsymbol{\xi}_i\right) \tag{13}$$

where $\boldsymbol{\xi}_i$ is the ith standard unit vector in $\mathbb{R}^{m_b}$. Further, the formula of $\boldsymbol{\alpha}$ can be written as

$$\boldsymbol{\alpha} = diag\left(\Sigma_{by}^{-1}\right) \tag{14}$$

Substituting Eq. (12) into Eq. (11), we can obtain the revised sub-problem over $\boldsymbol{\lambda}$ as

$$\min_{\boldsymbol{\lambda}}\left\|ADY - \frac{G}{\sqrt{n_p}}\right\|_{\Sigma_n}^2 + \boldsymbol{\alpha}^T\boldsymbol{\lambda} = \sum_{i=1}^{m_b}\left(\frac{\bar{q}_i^2}{\lambda_i} + \alpha_i\lambda_i\right) \tag{15}$$

where $\bar{q}_i$ denotes the ith element of $\bar{\boldsymbol{q}} = diag(QQ^T) = [\bar{q}_1, ..., \bar{q}_{m_b}]^T$, $Q = ADY - G/\sqrt{n_p}$. Since $\boldsymbol{\lambda} \geq 0$, the solution over $\boldsymbol{\lambda}$ is

$$\lambda_i^{new} = \sqrt{\frac{\bar{q}_i^2}{\alpha_i}}. \tag{16}$$

3. More Experimental Results

In this section, we provide more experimental results on the orthogonal transformation based HCS and dictionary based HCS.

3.1. Performance Evaluation on Orthogonal Transformation Based HCS

Given Haar wavelet as linear basis matrix D , we conduct OMP [9], StOMP [5], LASSO [6], FL [1], RCS [4] and the proposed RLPHCS to reconstruct the HSI from the linear measurements G, which is corrupted with additive Gaussian white noise. The HSI comes from three real hyperspectral datasets, namely INDIANA, URBAN and PAVIAU. Figure 1 and Figure 2 give the visual reconstruction results of all competing methods with sampling rate $\rho = 0.2$ when SNR of measurements is $10db$ and $30db$.

The results in Figure 1 and Figure 2 indicate that the proposed RLPHCS has the most approximate visual reconstruction results among all methods. This conclusion is consistent with those in the main paper.

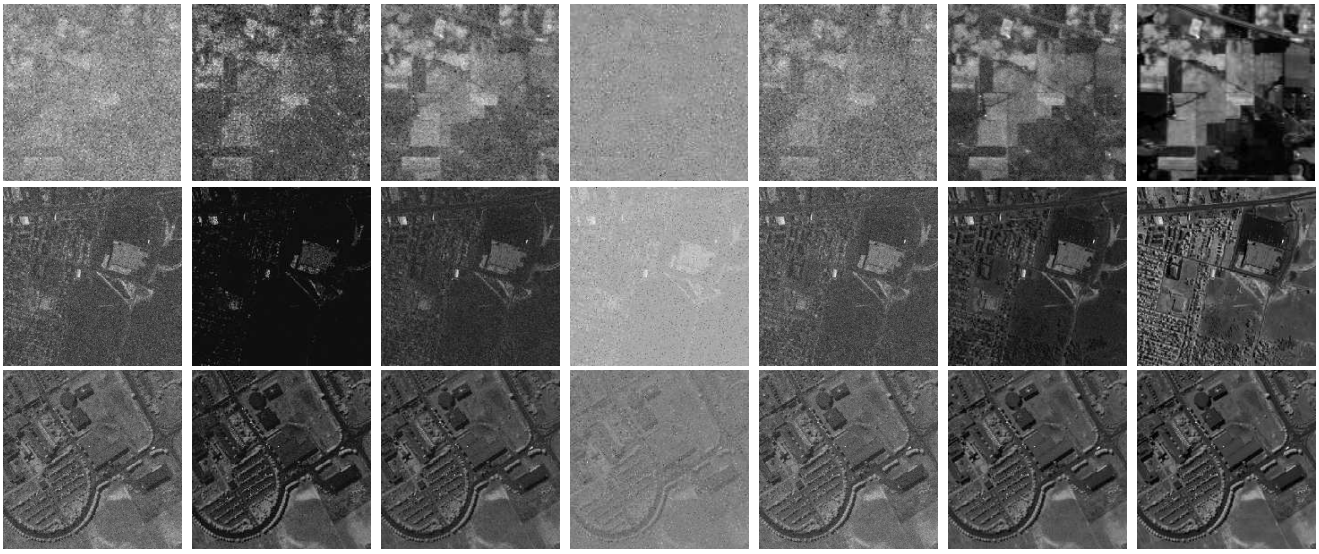

(a) (b) (c) (d) (e) (f) (g)

Figure 1. Visual reconstruction results of the 20th band from INDIANA, the 60th band from URBAN and the 90th band from PAVIAU with sampling rate $\rho = 0.2$ when SNR of measurements is $10db$. All the comparison methods recover the HSI in a wavelet transform based HCS framework. (a) OMP, (b) StOMP, (c) Lasso, (d) FL, (e) RCS, (f) RLPHCS, (g) Original bands.

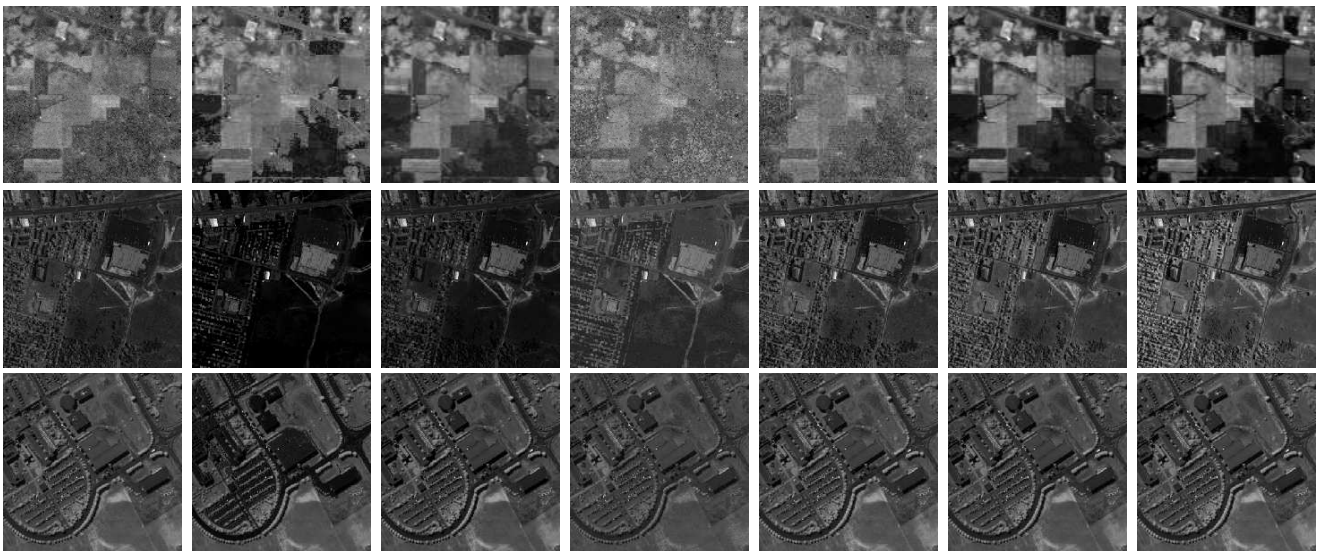

(a) (b) (c) (d) (e) (f) (g)

Figure 2. Reconstruction results of the 20th band from INDIANA, the 60th band from URBAN and the 90th band from PAVIAU with sampling rate $\rho = 0.2$ when SNR of measurements is $30db$. All the comparison methods recover the HSI in a wavelet transform based HCS framework. (a) OMP, (b) StOMP, (c) Lasso, (d) FL, (e) RCS, (f) RLPHCS, (g) Original bands.

3.2. Performance Evaluation on Dictionary Based HCS

In hyperspectral domain, the HSI can be linearly represented by a spectrum dictionary where each spectrum in the dictionary is termed as an endmember. Given 100 endmembers [2] extracted from each HSI by NFINDR [10] as the dictionary D to transform the HSI into a sparse matrix Y, OMP [9], StOMP [5], LASSO [6], UCS [7] and HYCA [8] are adopted as the comparison methods to reconstruct HSI with sampling rate ρ ranging from 0.01 to 0.09. To simulate the random noise in compressive sensing procedure, we add Gaussian white noise to the measurements, which results in the SNR of measurements to be $10db$ and $20db$. Similar to the main paper, INDIANA, URBAN and PAVIAU are employed as the test data. Three

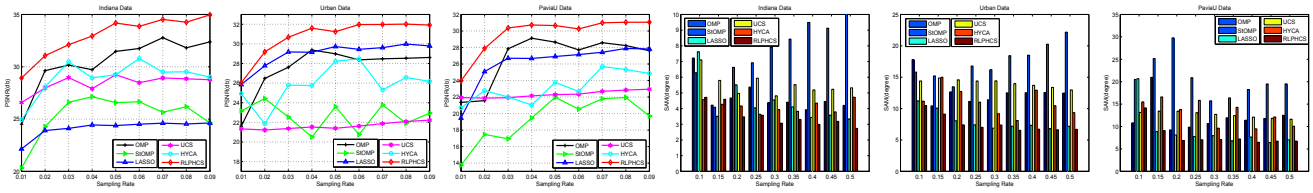

(a) (b) (c) (d) (e) (f)

Figure 3. The PSNR curves and SAM bar charts of different methods on three datasets under SNR=10db. (a)(b)(c) PNSR curves. (d)(e)(f) SAM bar charts.

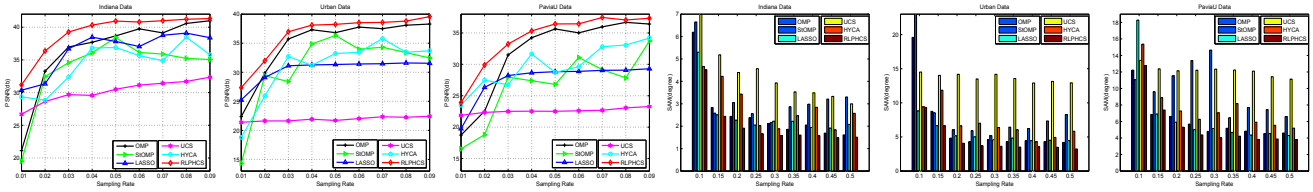

(a) (b) (c) (d) (e) (f)

Figure 4. The PSNR curves and SAM bar charts of different methods on three datasets under SNR=20db. (a)(b)(c) PNSR curves. (d)(e)(f) SAM bar charts.

Table 1. The SSIM scores of different methods on three datasets under SNR = 10db.

Results on INDIANA dataset									
	$\rho = 0.01$	$\rho = 0.02$	$\rho = 0.03$	$\rho = 0.04$	$\rho = 0.05$	$\rho = 0.06$	$\rho = 0.07$	$\rho = 0.08$	$\rho = 0.09$
OMP [9]	**0.8337**	0.7720	0.7628	0.7195	0.7750	0.7873	0.8081	0.7822	0.7969
StOMP [5]	0.7131	0.8118	0.6278	0.5969	0.5849	0.5775	0.5178	0.5437	0.4625
LASSO [6]	0.8024	0.8331	0.8420	0.8636	0.8595	0.8587	0.8597	0.858	0.8597
UCS [7]	0.7643	0.7908	0.8066	0.7993	0.8209	0.8114	0.8235	0.8266	0.8261
HYCA [8]	0.6679	0.6811	0.8012	0.7230	0.7441	0.7931	0.7518	0.746	0.7383
RLPHCS	0.8090	**0.8836**	**0.8753**	**0.9051**	**0.9217**	**0.9226**	**0.9260**	**0.9278**	**0.9253**
Results on URBAN dataset									
	$\rho = 0.01$	$\rho = 0.02$	$\rho = 0.03$	$\rho = 0.04$	$\rho = 0.05$	$\rho = 0.06$	$\rho = 0.07$	$\rho = 0.08$	$\rho = 0.09$
OMP [9]	0.7147	0.7476	0.7410	0.7923	0.7763	0.7573	0.7602	0.7728	0.7676
StOMP [5]	0.6583	0.6291	0.6595	0.5652	0.6307	0.6000	0.6156	0.5803	0.5503
LASSO [6]	**0.8425**	0.8423	0.8893	0.8895	0.9107	0.9006	0.9015	0.9143	0.9050
UCS [7]	0.3738	0.3818	0.3986	0.4162	0.4166	0.4350	0.4556	0.4758	0.4933
HYCA [8]	0.6653	0.4837	0.6714	0.6622	0.7915	0.7915	0.6462	0.7193	0.687
RLPHCS	0.7364	**0.8787**	**0.9093**	**0.9300**	**0.9255**	**0.9289**	**0.9309**	**0.9353**	**0.9288**
Results on PAVIAU dataset									
	$\rho = 0.01$	$\rho = 0.02$	$\rho = 0.03$	$\rho = 0.04$	$\rho = 0.05$	$\rho = 0.06$	$\rho = 0.07$	$\rho = 0.08$	$\rho = 0.09$
OMP [9]	0.6414	0.7250	0.7392	0.7635	0.7476	0.7035	0.7481	0.7371	0.719
StOMP [5]	0.5002	0.4076	0.4086	0.4933	0.5692	0.5619	0.5242	0.537	0.5268
LASSO [6]	0.645	0.7693	0.7963	0.8229	0.8249	0.8413	0.8376	0.8531	0.8605
UCS [7]	0.4207	0.4305	0.4406	0.4600	0.4734	0.4815	0.5061	0.5203	0.5313
HYCA [8]	0.3954	0.5357	0.5372	0.5350	0.5673	0.5701	0.6111	0.6009	0.5697
RLPHCS	**0.6735**	**0.7973**	**0.8712**	**0.8801**	**0.8823**	**0.8838**	**0.8835**	**0.8862**	**0.8899**

evaluation measures including PSNR, SAM and SSIM, are utilized to evaluate the reconstruction performance, which record the average performance of each method after 10 Monte-Carlo runs, including PSNR, SAM and SSIM.

Under two levels of noise, the results of PSNR and SAM on three datasets are shown in Figure 3 and Figure 4, respectively. It is clear that the proposed RLPHCS gives the highest PSNR among all comparison methods. The SAM values of the proposed RLPHCS are lower than those of other methods in most cases. Additionally, the SSIM scores on three datasets are given in Table 1 and Table 2. Under two different levels of noise, it can be seen that the proposed RLPHCS gives the highest SSIM scores in most cases. The results evaluated by three measures indicate that the proposed RLPHCS outperforms other methods on the reconstruction accuracy of HSI with the dictionary based sparsification strategy.

References

[1] S. D. Babacan, R. Molina, and A. K. Katsaggelos. Bayesian compressive sensing using laplace priors. *Image Processing, IEEE Transactions on*, 19(1):53–63, 2010.

Table 2. The SSIM scores of different methods on three datasets under SNR = $20db$.

Results on INDIANA dataset									
	$\rho = 0.01$	$\rho = 0.02$	$\rho = 0.03$	$\rho = 0.04$	$\rho = 0.05$	$\rho = 0.06$	$\rho = 0.07$	$\rho = 0.08$	$\rho = 0.09$
OMP [9]	0.8448	0.9405	0.9579	0.9654	0.9699	0.97	0.975	0.9722	0.9721
StOMP [5]	0.8599	0.8985	0.8644	0.8895	0.9338	0.8972	0.8863	0.8784	0.8699
LASSO [6]	**0.9432**	0.9564	0.9726	**0.9778**	0.9763	0.975	**0.9800**	**0.9796**	**0.9785**
UCS [7]	0.766	0.7983	0.8168	0.823	0.8389	0.8512	0.859	0.8662	0.8758
HYCA [8]	0.8396	0.7871	0.862	0.9365	0.934	0.9219	0.9017	0.9532	0.9161
RLPHCS	0.9085	**0.9583**	**0.9727**	0.9751	**0.9780**	**0.9771**	0.9785	0.9785	0.979
Results on URBAN dataset									
	$\rho = 0.01$	$\rho = 0.02$	$\rho = 0.03$	$\rho = 0.04$	$\rho = 0.05$	$\rho = 0.06$	$\rho = 0.07$	$\rho = 0.08$	$\rho = 0.09$
OMP [9]	0.7574	0.9148	0.9603	0.9675	0.9590	0.9680	0.9656	0.9663	0.9665
StOMP [5]	0.2382	0.895	0.9135	0.9318	0.9461	0.9139	0.9233	0.8992	0.8815
LASSO [6]	0.8684	0.9241	0.9479	0.9516	0.9549	0.9523	0.9563	0.9577	0.9576
UCS [7]	0.3778	0.3992	0.4107	0.4365	0.4347	0.4591	0.4839	0.4862	0.5017
HYCA [8]	0.5687	0.7464	0.9137	0.8648	0.9265	0.9248	0.9543	0.9206	0.9253
RLPHCS	**0.8937**	**0.9473**	**0.9770**	**0.9806**	**0.9817**	**0.9821**	**0.9822**	**0.9825**	**0.9851**
Results on PAVIAU dataset									
	$\rho = 0.01$	$\rho = 0.02$	$\rho = 0.03$	$\rho = 0.04$	$\rho = 0.05$	$\rho = 0.06$	$\rho = 0.07$	$\rho = 0.08$	$\rho = 0.09$
OMP [9]	0.6595	0.8278	0.9184	0.9411	0.9406	0.9287	0.9412	0.9464	0.9441
StOMP [5]	0.3720	0.5811	0.7622	0.7179	0.6809	0.9006	0.8343	0.8404	0.8976
LASSO [6]	0.7331	0.8810	0.8899	0.9012	0.9070	0.9075	0.9161	0.9185	0.9218
UCS [7]	0.4193	0.4501	0.4684	0.4812	0.4853	0.4964	0.5088	0.5327	0.5496
HYCA [8]	0.7171	0.8467	0.6827	0.8848	0.8395	0.7951	0.9145	0.8927	0.9153
RLPHCS	**0.7838**	**0.9096**	**0.9377**	**0.9533**	**0.9631**	**0.9621**	**0.9666**	**0.9639**	**0.9657**

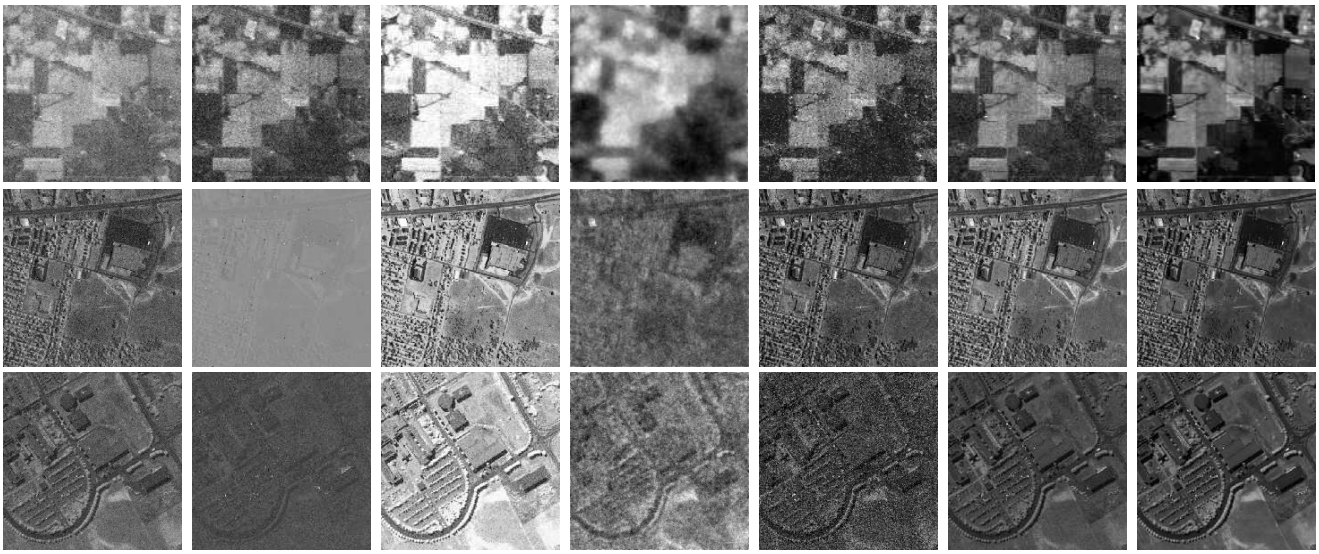

(a) (b) (c) (d) (e) (f) (g)

Figure 5. Reconstruction results of the 20th band from INDIANA, the 60th band from URBAN and the 90th band from PAVIAU with sampling rate $\rho = 0.2$ when SNR of measurements is $10db$. All the comparison methods recover the HSI in a dictionary based HCS framework. (a) OMP, (b) StOMP, (c) Lasso, (d) FL, (e) RCS, (f) RLPHCS, (g) Original bands.

[2] J. Bioucas-Dias and A. Plaza. Hyperspectral unmixing: Geometrical, statistical, and sparse regression-based approaches. In *Proc. SPIE*, volume 7830, page 78300A, 2010.

[3] S. Boyd and L. Vandenberghe. *Convex optimization*. Cambridge university press, 2004.

[4] E. J. Candes, M. B. Wakin, and S. P. Boyd. Enhancing sparsity by reweighted l1 minimization. *Journal of Fourier analysis and applications*, 14(5-6):877–905, 2008.

[5] D. L. Donoho, Y. Tsaig, I. Drori, and J.-L. Starck. Sparse solution of underdetermined systems of linear equations by stagewise orthogonal matching pursuit. *Information Theory, IEEE Transactions on*, 58(2):1094–1121, 2012.

[6] B. Efron, T. Hastie, I. Johnstone, R. Tibshirani, et al. Least angle regression. *The Annals of statistics*, 32(2):407–499, 2004.

[7] C. Li, T. Sun, K. F. Kelly, and Y. Zhang. A compressive sensing and unmixing scheme for hyperspectral data processing. *Image Processing, IEEE Transactions on*, 21(3):1200–1210, 2012.

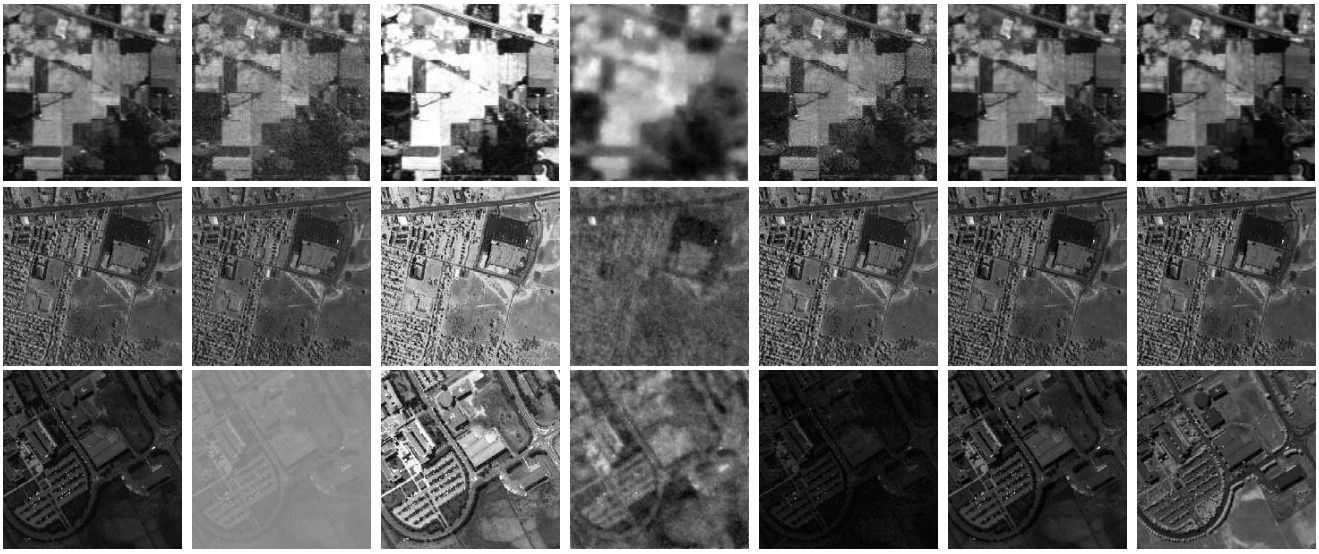

(a) (b) (c) (d) (e) (f) (g)

Figure 6. Reconstruction results of the 20th band from INDIANA, the 60th band from URBAN and the 90th band from PAVIAU with sampling rate $\rho = 0.2$ when the SNR of measurements is $20db$. All the comparison methods recover the HSI in a dictionary based HCS framework. (a) OMP, (b) StOMP, (c) Lasso, (d) FL, (e) RCS, (f) RLPHCS, (g) Original bands.

[8] G. Martin, J. M. Bioucas-Dias, and A. Plaza. Hyperspectral coded aperture (hyca): A new technique for hyperspectral compressive sensing. In *Signal Processing Conference (EUSIPCO), 2013 Proceedings of the 21st European*, pages 1–5. IEEE, 2013.

[9] J. A. Tropp and A. C. Gilbert. Signal recovery from random measurements via orthogonal matching pursuit. *Information Theory, IEEE Transactions on*, 53(12):4655–4666, 2007.

[10] M. E. Winter. N-findr: an algorithm for fast autonomous spectral end-member determination in hyperspectral data. In *SPIE's International Symposium on Optical Science, Engineering, and Instrumentation*, pages 266–275. International Society for Optics and Photonics, 1999.